NUMERICAL STUDY OF SLIP AND RADIATIVE IMPACT ON MAGNETIC FE₃O₄-WATER-BASED NANOFLUID FLOW FROM A NONLINEAR POROUS STRETCHING PLATE WITH SORET AND DUFOUR DIFFUSION

M. M. BHATTI*
College of Mathematics/Systems Science, Shandong University of Science and Technology, Shandong, 266590, China
Shanghai Institute of Applied Mathematics and Mechanics, Shanghai University, Shanghai 200072, China
International Institute of Symmetry Analysis and Mathematical modeling, Department of Mathematical Sciences,
North West University, Mafikeng Campus, Mmabatho, South Africa
*Corresponding author- Email: muhammad09@shu.edu.cn
C. M. KHALIQUE
International Institute of Symmetry Analysis and Mathematical modeling, Department of Mathematical Sciences,
North West University, Mafikeng Campus, Mmabatho, South Africa
TASVEER A. BÉG
Renewable Energy and Multi-Physics Research, Israfil House, Dickenson Road, Manchester, M13, UK.
O. ANWAR BÉG and ALI KADIR
*Multi-Physical Fluid Dynamics, Mechanical/Aero Engineering, Salford University, Manchester, M54WT, **UK**.*
Emails: tasveerabeg@gmail.com; O.A.Beg@salford.ac.uk; A.Kadir@salford.ac.uk

Abstract: Increasingly sophisticated techniques are being developed for the manufacture of functional nanomaterials. A growing interest is also developing in magnetic nanofluid coatings which contain magnetite nano-particles suspended in a base fluid and are responsive to external magnetic fields. These nanomaterials are "smart" and their synthesis features high-temperature environments in which radiative heat transfer is present. Diffusion processes in the extruded nano-material sheet also feature Soret and Dufour (cross) diffusion effects. Filtration media are also utilized to control the heat, mass and momentum characteristics of extruded nano-materials and porous media impedance effects arise. Magnetite nanofluids have also been shown to exhibit hydrodynamic wall slip which can arise due to non-adherence of the nanofluid to the boundary. Motivated by the multi-physical nature of magnetic nanomaterial manufacturing transport phenomena, in the present article we develop a mathematical model to analyze the collective influence of hydrodynamic slip, radiative heat flux and cross-diffusion effects on transport phenomena in ferric oxide (Fe_3O_4- water) magnetic nanofluid flow from a nonlinear stretching porous sheet in porous media. Hydrodynamic slip is included. Porous media drag is simulated with the Darcy model. Viscous magnetohydrodynamic theory is used to simulate Lorentzian magnetic drag effects. The Rosseland diffusion flux model is employed for thermal radiative effects. A set of appropriate similarity transformation variables are deployed to convert the original partial differential boundary value problem into an ordinary differential boundary value problem. The numerical solution of the coupled, multi-degree, nonlinear problem is achieved with an efficient shooting technique in MATLAB symbolic software. The physical influence of Hartmann (magnetic) number, Prandtl number, Richardson number, Soret (thermo-diffusive) number, permeability parameter, concentration buoyancy ratio, radiation parameter, Dufour (diffuso-thermal) parameter, momentum slip parameter and Schmidt number on transport characteristics (e.g. velocity, nanoparticle concentration and temperature profiles) are investigated and visualized presented graphically. Flow deceleration is induced with increasing Hartmann number and wall slip whereas flow acceleration is generated with greater Richardson number and buoyancy ratio parameter. Temperatures are elevated with increasing Dufour number and radiative parameter. Concentration magnitudes are enhanced with Soret number whereas they are depleted with greater Schmidt number. Validation of the MATLAB computations with special cases of the general model is included. Further validation with generalized differential quadrature is also included.

Keywords: *Hydrodynamic **s**lip; magnetic nanofluid; Nonlinear sheet; Radiative heat transfer; Shooting method; Mass transfer; Cross diffusion; smart nanomaterial processing; MATLAB; GDQ method*.
NOMENCLATURE

$\tilde{p}$	Pressure
Re	Reynolds number
$\tilde{t}$	Time
$\hat{x}, \hat{y}$	Cartesian coordinates
P_r	Prandtl number
u_s	Slip velocity
$\tilde{u}, \tilde{v}$	Velocity components
C	Nanoparticle concentration
$\tilde{T}_m$	Mean fluid temperature
$K_{\tilde{T}}$	Thermal diffusivity ratio
v_w	Wall mass flux
J	Current density
S_c	Schmidt number
S	Suction/injection parameter
S_r	Soret number
D_u	Dufour number
$\tilde{T}_w$	Sheet temperature
$\tilde{T}_\infty$	Environmental (ambient) temperature
M	Hartmann number
c_s	Concentration susceptibility
k	Darcy drag parameter
g	Gravity
$\bar{k}$	Mean absorption coefficient
c_p	Specific heat
C_1, C_2, C_3	Positive constants
Ri	Richardson number
B	Magnetic field vector
Sh_r	Sherwood number

Greek Symbols

$\bar{\alpha}$	Thermal conductivity
η	Concentration buoyancy ratio
$\beta*$	Thermal expansion coefficient
β	Hydrodynamic slip parameter
$\bar{\sigma}$	Stefan-Boltzmann constant
ρ_{nf}	Density of nanofluid
$\hat{\varphi}$	Stream function
Φ	Dimensionless nanoparticle concentration
θ	Dimensionless temperature
μ_{nf}	Viscosity of nanofluid
σ	Electrical conductivity of nanofluid
ν_{nf}	Kinematic viscosity of nanofluid

1. INTRODUCTION

The simultaneous heat and mass transfer from a nonlinear stretching surface is a fundamental problem in modern extrusion manufacturing processes. It features extensively in the synthesis of plastics, cooling of metallic plates in power transportation and electronic devices and also in numerous coating surface treatment technologies. Many manufacturing processes generate considerable heat and to regulate thermal fields frequently a number of cooling techniques are required. These typically feature perforated walls (transpiration cooling) [1], air current blowing over the surface of the extruded sheet, heat extraction devices (sinks) etc. Traditional heat transfer liquids which include water, engine oil and ethylene glycol (often the base fluid in nano-polymeric materials) have a very poor capability to transfer heat. To overcome this difficulty, engineers in the 1990s explored (at Argonne Energy Laboratory in the USA), a novel approach of adding nanoparticles (size: 1-100nm) to base fluids. The resulting combined colloidal suspensions were termed nanofluids, as defined by Choi [2]. In comparison with milli- and micro- sized particle suspensions explored in past, the nanoparticles are closer in molecular dimension to the particles of the base fluid. Nanofluids have been shown to exhibit high, non-linear and anomalous thermal conductivity, compared to the base fluid and to achieve significant elevations in heat transfer rates.

Nanofluid dynamics involves four scales: the *molecular scale, the microscale, the macroscale* and *the mega-scale* and an interaction is known to take place between these scales. Diverse types of nanofluids can be synthesized by combining different nano-particles (e.g. metallic oxides, silicon carbides, carbon nanotubes) with different base fluids. Nanofluids have been utilized in many diverse applications including biomedical engineering (drug delivery, biological sensors, anti-bacterial coatings [3]), transportation (fuels cells, propellants, lubricants, anti-fouling coatings) and energy systems (solar and magnetohydrodynamic power generation, solar collector coatings [4] etc). The considerable enhancement in thermal efficiency achieved with nanofluids has made them the focus of significant research, both from a computational and experimental view point. Several interesting studies of nanofluid stretching sheet transport modelling have been communicated in recent years focused on the complex hydrodynamics of sheet extrusion and interaction of nanoscale effects with boundary layer behaviour. These studies have considered multiple effects including magnetohydrodynamics, multi-mode heat transfer, different metallic nano-particles. Since mathematical models of nanofluid sheet stretching are inherently non-linear, many studies have also deployed an extensive range of simulation techniques (numerical methods).

A sub-branch of nanofluids which contain magnetized or ferro-suspensions are known as magnetic nanofluids. They are a special case of ferrofluids. Frequently iron oxide nano-particles are utilized with aqueous base fluid and the resulting magnetic nanofluids can be characterized accurately with a variety of methods including Fourier transform infrared spectroscopy, X-ray diffraction and transmission electronic microscopy. The elevation in electrical conductivity of magnetic nanofluids with increasing volume fractions and temperatures has been verified by Bagheli *et al.* [5]. Extensive applications of magnetic nanofluids in thermal devices, power systems and coating systems have been documented by Nkurikiyimfura *et al.* [6]. These studies have also shown that magnetic nanofluids are in fact state-of-the art *smart or functional fluids* in engineering. The thermal enhancement characteristics achieved with magnetic nanofluids in natural and forced convection and boiling (phase change) systems have also been confirmed by Bahairaie and Hangi [7]. Jia *et al.* [8] investigated the behaviour of ferrofluids (magnetic nanofluids) in heat transfer systems and observed that greater heat convective heat transfer rates are achieved with careful nano-particle doping and that the ferrofluid behaves as a thermal magnetohydrodynamic one i.e. it is responsive to external magnetic field. Magnetohydrodynamic nanofluid dynamics [9] therefore provides a sensible framework for analyzing the hydrodynamics of magnetic nanofluids

in which Lorentzian magnetic body forces, magnetic flux, Ohmic dissipation (Joule heating), Hall currents, magnetic boundary layer thickness and ion slip among other phenomena arise.

The study of boundary layer stretching flows of continuous sheets was mobilized as a rich area of viscous hydrodynamics research by Sakiadis [10]. It was further studied by Crane [11] although for the linear stretching sheet case in which polymer is extruded from a slit with a linear velocity. More recently magnetic nano-polymeric sheet stretching in manufacturing processes has been considered by Müller [12] for various sectors including aerospace components, medical prosthetics, solar collector coatings etc. Guo *et al*. [13] have also elaborated on the complex fluid dynamics inherent to sheet stretching of nano-liquids and nano-composite gels, identifying the "green" and environmentally-friendly nature of this technology. These developments have in turn motivated extensive activity in mathematical modelling of magnetic nanofluid sheet stretching flows with a rich variety of computational algorithms. Mabood *et al.* [14] presented homotopy solutions for magnetic nanofluid boundary layer flow in a stretching sheet regime with a quadratic stretching velocity. Bég *et al*. [15] reported on explicit finite difference solutions for both free and forced convection heat transfer in time-dependent exponential stretching of a magnetic nanofluid in a homogenous permeable material. Abbas *et al.* [16] used a numerical shooting procedure to study the stretching of a magnetic nanofluid (comprising copper or silver nano-particles in water base fluid) over a curved surface. Thumma *et al.* [17] conducted finite element simulations to evaluate the viscous heating and also heat generation/absorption effects in magnetic nanofluid boundary layer flow from both an inclined extending and contracting sheet.

In many nano-polymer manufacturing processes, *slip phenomena* can arise at the stretching surface. Since magnetic nanofluids contain minute particles, the *no-slip* boundary condition traditionally employed in boundary layer models is inadequate. Slip effects can arise in rarefied gases (e.g. hypersonic flows where the continuum approximation breaks down) and polymeric fluids with high elastic properties. Slippage arising in nano-polymers exhibits significant tangential traction and non-adherence of the stretching sheet can dramatically modify thermo-fluid characteristics. A number of investigators have addressed slip phenomena in magnetic nanofluid (ferrofluid) stretching/shrinking sheet simulations. Nandy and Mahaparta [18] considered the hydrodynamic slip effects on magnetic nanofluid stretching/shrinking sheet flow with thermophysical effects, observing that for the stretching sheet, flow deceleration is induced with greater wall slip and magnetic field whereas temperature and nanoparticle concentration

magnitudes are boosted. Ayub *et al.* [19] investigated electrical and magnetic field effects in slip flow of nanofluids in a Riga plate (magnetic actuator) system. Uddin *et al.* [20] studied magnetic nanofluid stretching/shrinking flows with Maple quadrature and Navier slip and convective heating boundary conditions. Shukla *et al.* [21] studied the impact of linear and quadratic hydrodynamic wall slip on entropy generation in magnetic nanofluid mixed convection from a a vertical cylinder, noting that entropy is enhanced with magnetic field, quadratic slip and curvature parameter whereas it is depressed with linear slip parameter. They also observed that Nusselt number is elevated with linear (first order) wall slip whereas it is reduced with quadratic slip. Further studies of slip magnetic nanofluid stretching flows have been reported by Hakeem *et al.* [22], Amrisom *et al.* [23] (including melting and bioconvection effects), Alkahtani *et al.* [24] (stagnation flow) and Uddin *et al.* [25] (for Falkner-Skan magnetic induction bio-nanofluid flows with thermal, nano-particle slip and micro-organism slip).

In high temperature materials processing, *radiative heat transfer* arises in conjunction with thermal conduction and thermal convection. The optical and radiative properties of magnetic nanofluids therefore have been studied extensively. Said *et al.* [26] have observed that composite nanofluid attain different thermophysical properties to either the base fluid or the nano-particles. Radiative properties of iron oxide (Fe_3O_4) nanoparticles (for magnetic nanofluids) have been examined via powder X-ray diffraction (XRD), transmission electron microscopy (TEM), vibrating sample magnetometry (VSM), dynamic light scattering (DLS) and theromo-gravimetrics by Shima *et al.* [27]. They have shown that thermal conductivity and radiative absorption of aqueous nanofluids increases with temperature while it shows a decrease in non-aqueous nanofluids. Thermal radiative heat transfer is therefore expected to be important in the synthesis of magnetic nano-polymers. To simulate radiative flux many approaches are available. The most general is the general integro-differential equation of radiative heat transfer. This provides the full details for radative behavior at different spectra and wavelengths. However, it is very challenging computationally and usually Monte Carlo or discrete ordinate techniques are required for solutions. Simpler approaches feature an *algebraic flux approximation* which may be (in progressively increasing complexity) of the Rosseland type, Milne-Eddington type, Schuster-Schwartzchild type, Traugott P1 flux model, Hamaker six flux model etc. In multi-physical nanofluid dynamics, the most pragmatic approach is the Rosseland model which is reasonably accurate for high optical thicknesses associated with magnetic nano-liquids (ferrofluids). Bhatti *et al.* [28] conducted a second law thermodynamic

analysis on radiative heat transfer in Carreau rheological magnetic nanofluid stretching sheet flow using the Rosseland diffusion flux approximation and a Chebyshev spectral collocation method. They noted that temperatures are enhanced with thermal radiation effect whereas they are reduced with Prandtl number. Zeeshan *et al.* [29] also used the Rosseland flux model to investigate the impact of magnetic dipole and thermal radiation on dimensionless velocity, temperature, pressure, skin friction and Nusselt number in magnetic dipole viscous ferro-fluid stretching flow. Further studies of radiative magnetic nanofluid flows include Bhatti *et al.* [30] (for both shrinking/expanding sheets), Haq *et al.* [31] (for slip stagnation stretching flows), Prakash *et al.* [32] (for peristaltic stretching tube smart pump flows) and Bhatti *et al.* [33] (for viscoelastic nanofluid expanding/contracting sheet flows).

The objective of the current study is to examine the *collective effects of Soret and Dufour cross diffusion, wall slip and radiative heat transfer* on Fe_3O_4 -water magnetic nanofluid flow from a nonlinear stretching/shrinking porous sheet adjacent to a Darcian porous medium. The nonlinear transformed ordinary differential boundary value problem is solved with an efficient shooting technique in MATLAB symbolic software [34]. A numerical comparison is also made with the previous published data in references [35]-[39] and excellent correlation is achieved. Further validation with a generalized differential quadrature method (GDQ) [40] is also included. The novelty of the current work is the simultaneous inclusion of Soret and Dufour effects, wall slip which are known to have a significant influence in magnetic materials processing [41-43]. The Dufour effect relates to the energy flux due to a species concentration gradient occurring and is the reciprocal phenomenon to the Soret effect. Both effects exert some influence on heat, mass and momentum characteristics in sheet processing, as elaborated in due course. The current investigation constitutes a novel contribution to the scientific literature on nanomaterial fabrication process simulation.

2. MATHEMATICAL FORMULATION

The regime under investigation comprises the two-dimensional, steady, incompressible boundary layer flow of a magnetic nanofluid from a vertical nonlinear porous stretching sheet at the stagnation point $y = 0$. An external magnetic field with strength, B_0, is applied transverse to the sheet. Magnetic Reynolds number is very small and induced magnetic field is therefore ignored. A Cartesian coordinate system is elected in which the $\hat{x}$-axis is orientated in the direction

of the sheet extrusion and the $\hat{y}$-axis is directed normal to it (see. Fig. (1)). The concentration and temperature at the sheet is $\tilde{C}_w$ and $\tilde{T}_w$ whereas the ambient concentration and temperature is $\tilde{C}_\infty$ and $\tilde{T}_\infty$. We considered the stretching velocity to be of the following *power-law* (nonlinear) form: $u_w(\hat{x}) = \pm C_1 \hat{x}^{2m}$. Thermal dispersion and stratification effects in the porous medium are neglected. Momentum slip occurs at the wall.
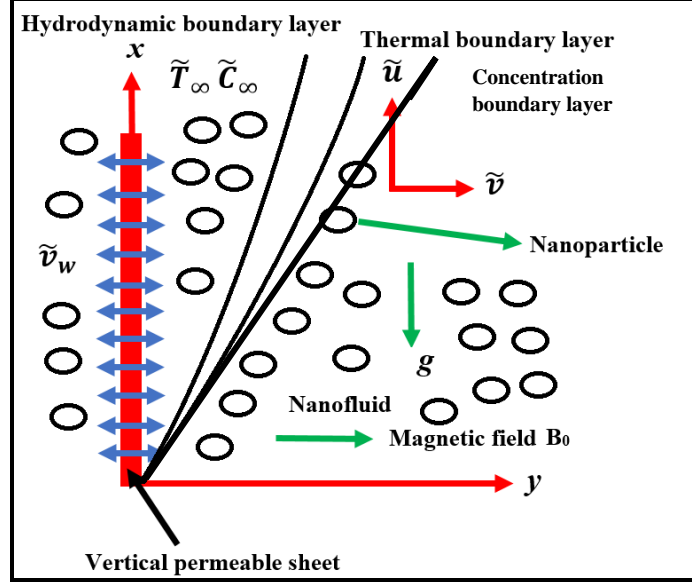
Fig. 1. Structure of the flow problem.

The governing equations for buoyancy-driven boundary layer flow of a magnetic nanofluid (ferrofluid) from a shrinking/stretching vertical sheet in a porous medium, are the mass, momentum, energy and nanoparticle concentration equations which are formulated by amalgamating the models in [26], [30] and [41]:

$$\frac{\partial \tilde{u}}{\partial \hat{x}} + \frac{\partial \tilde{v}}{\partial \hat{y}} = 0, \tag{1}$$

$$\frac{\partial \tilde{u}}{\partial \hat{x}}\tilde{u} - \frac{\mu_{nf}}{\rho_{nf}}\left[\frac{\partial^2 \tilde{u}}{\partial \hat{y}^2}\right] = -\frac{\mu_{nf}}{\rho_{nf}\bar{k}}\tilde{u} + \mathbf{J}\times\mathbf{B} + \left(\tilde{T}-\tilde{T}_\infty\right)\frac{(\rho\beta_{\tilde{T}})_{nf}}{\rho_{nf}}\bar{g} - \tilde{v}\frac{\partial \tilde{v}}{\partial \hat{y}} + \left(\tilde{C} - \tilde{C}_\infty\right)\frac{(\rho\beta_{\tilde{C}})_{nf}}{\rho_{nf}}\bar{g}, \tag{2}$$

$$\tilde{v}\frac{\partial \tilde{T}}{\partial \hat{y}} - \frac{D_m K_{\tilde{T}}}{c_s c_p}\frac{\partial^2 \tilde{C}}{\partial \hat{y}^2} - \bar{\alpha}\frac{\partial^2 \tilde{T}}{\partial \hat{y}^2} = -\frac{1}{\rho c_p}\frac{\partial}{\partial \hat{y}}\left[-\frac{16\bar{\sigma}\tilde{T}^3}{3\bar{k}}\frac{\partial \tilde{T}}{\partial \hat{y}}\right] - \tilde{u}\frac{\partial \tilde{T}}{\partial \hat{x}}, \tag{3}$$

$$\tilde{u}\frac{\partial \tilde{C}}{\partial \hat{x}} - \frac{D_m K_{\tilde{T}}}{\tilde{T}_m}\frac{\partial^2 \tilde{C}}{\partial \hat{y}^2} = D_m\frac{\partial^2 \tilde{T}}{\partial \hat{y}^2} - \tilde{v}\frac{\partial \tilde{C}}{\partial \hat{y}}, \tag{1}$$

The associated boundary conditions become:

$$\tilde{u}(0) = u_w(\hat{x}) + u_s, \tilde{v}(0) = v_w, \tilde{T}(0) = \tilde{T}_\infty + C_2\hat{x}^{2m-1}, \tilde{C}(0) = \tilde{C}_\infty + $$
$$C_3\hat{x}^{2m-1}, \tag{6}$$

$$\tilde{T}(\infty) = \tilde{T}_\infty, \tilde{u}(\infty) \to 0, \tilde{C}(\infty) = \tilde{C}_\infty. \tag{7}$$

It is important to note that a wall transpiration velocity, v_w (>0 for suction and < 0 for blowing) is included in the velocity wall boundary condition (6). A dimensional stream function can be described as follows:

$$\tilde{u} = \frac{\partial \hat{\varphi}}{\partial \hat{y}}, \tilde{v} = -\frac{\partial \hat{\varphi}}{\partial \hat{x}}. \tag{8}$$

Similarity transformation variables are then defined in order to normalize the governing partial differential boundary value problem:

$$\zeta = \sqrt{\frac{(m+1)\hat{y}^2 u_w(\hat{x})}{2v_f\hat{x}}}, \varphi = \sqrt{\frac{2\hat{x}v_f u_w(\hat{x})}{(m+1)}}f, M = \frac{2B_0^2\sigma}{C_1\rho_{nf}u_w\hat{x}^{-1}(m+1)}, \theta = $$
$$\frac{\tilde{T}-\tilde{T}_\infty}{\tilde{T}_w-\tilde{T}_\infty}, P_r = \frac{v_f}{\bar{\alpha}_f}, \ \bar{\alpha}_f = \frac{\kappa_f}{\rho c_p}, \Phi = \frac{\tilde{C}-\tilde{C}_\infty}{\tilde{C}_w-\tilde{C}_\infty}, D_u = \frac{D_m K_{\tilde{T}}}{v_f c_s c_p}\left(\frac{\tilde{C}_w-\tilde{C}_\infty}{\tilde{T}_w-\tilde{T}_\infty}\right), S_c = $$
$$\frac{v_f}{D_m}, S_r = \frac{D_m K_{\tilde{T}}}{\tilde{T}_m v_f}, \eta = \frac{A_6(\rho\beta_{\tilde{C}})_{nf}}{A_4(\rho\beta_{\tilde{T}})_{nf}}\left(\frac{\tilde{C}_w-\tilde{C}_\infty}{\tilde{T}_w-\tilde{T}_\infty}\right), R_i = \frac{x(\rho\beta_{\tilde{T}})_{nf}}{\rho_{nf}u_w}\left(\tilde{T}_w - \tilde{T}_\infty\right), S = $$
$$-\frac{\tilde{v}_w}{(C_1 v_f)^{\frac{1}{2}}}, k = \frac{2v_{nf}}{(m+1)x^{-1}u_w\bar{k}}. \tag{9}$$

Using the variables in Eqn. (9) into Eqn. (1) to Eqn. (8), we arrive at the following 7th order system of multi-degree, coupled nonlinear ordinary differential equations:

$$\frac{1}{A_1 A_2}F''' - \frac{2m}{m+1}F'^2 + FF'' - \frac{A_5}{A_2}M^2 F' - \frac{k}{A_2}F'$$
$$+ \frac{2A_4}{(m+1)A_2}R_i(\theta + \eta\Phi) = 0, \tag{10}$$

$$\frac{A_6}{A_3 P_r}\theta'' + \frac{4R_d}{3A_3}\theta'' + F\theta' - \frac{2(2m-1)}{m+1}\theta F' + D_u\Phi'' = 0, \tag{11}$$

$$\Phi'' + S_C \Phi' F + 2(m+1)^{-1}(1-2m)S_C \Phi F' = -S_C S_r \theta''. \tag{12}$$

The associated non-dimensional boundary conditions at the sheet surface (wall) and in the free stream emerge as:

$$F(0) = S, \beta F''(0) = \pm 1 - F'(0), F'(\infty) = 0, \tag{13}$$

$$\Phi(0) = \theta(0) = 1, \tag{14}$$

$$\Phi(\infty) = \theta(\infty) = 0. \tag{15}$$

In the momentum Eqn. (10) when $M = 0$ magnetic drag force vanishes, and the electrically non-conducting case is retrieved. When $k = 0$, the Darcian drag force vanishes and the medium is purely nanofluid i.e. vanishing of porous medium fibers. When $Ri = 0$ (i.e. vanishing Richardson number) buoyancy effects are negated and the momentum equation is de-coupled from the energy and species equations. The momentum slip parameter, β, appears in the wall boundary condition (13). In the absence of slip, $\beta \rightarrow 0$ and we retrieve the conventional *no-slip* condition. In Eqns. (10)-(12) the following notation applies:

$$A_1 = (-\phi+1)^{2.5}, A_2 = 1 + \phi\left(\frac{\rho_s}{\rho_f}\right) - \phi, A_3 = 1 - \phi + \frac{\phi(\rho C_p)_s}{(\rho C_p)_f}, A_4 = 1 -$$
$$\phi + \frac{\phi(\rho\beta_{\tilde{T}})_s}{(\rho\beta_{\tilde{T}})_f}, A_5 = 1 - \frac{3(1-\tilde{\gamma})\phi}{(\tilde{\gamma}+2)+(1-\tilde{\gamma})\phi}, \tilde{\gamma} = \frac{\sigma_s}{\sigma_f}, A_6 = 1 - \phi + \frac{\phi(\rho\beta_{\tilde{C}})_s}{(\rho\beta_{\tilde{C}})_f}. \tag{16}$$

Here nano-particle volume fraction is designated as ϕ. In materials processing operations [44], important wall gradient functions include the surface shear stress, heat transfer rate and nano-particle mass transfer rate. These physical quantities in dimensionless form take the following definitions:

$$C_F = C_f \text{Re}_x^{1/2} = \frac{-2}{(1-\phi)^{2.5}}F''(0), Nu_r = \frac{Nu_x}{\text{Re}_x^{1/2}}$$
$$= -\frac{\kappa_{nf}}{\kappa_f}\left(1 + \frac{4}{3}R_d\right)\theta'(0), Sh_r = -\Phi'(0), \tag{17}$$

where C_F, Nu_r and Sh_r are the dimensionless skin friction coefficient, Nusselt number and Sherwood number. $\text{Re}_x = \tilde{u}_w \hat{x}/\nu$ is a local Reynolds number. These definitions are based on Hammad and Ferdows [35].

3. NUMERICAL SOLUTION OF NONLINEAR BOUNDARY VALUE PROBLEM

The emerging mathematical model features many control parameters i.e. *Hartmann number (M), Darcian drag force parameter (k), Richardson number (Ri), slip parameter (ξ), species to thermal buoyancy ratio (η), transpiration parameter (S), Schmidt number (Sc), Soret (thermo-diffusion) number (Sr), Dufour diffuso-thermal number (Du), Prandtl number (Pr), power-law stretching parameter (m), electrical conductivity ratio (γ).* Unless otherwise noted these parameters assume default values of unity. Only selected parameters are simulated. A numerical shooting method is applied to solve Eqns. (10) - (12) along with relevant boundary conditions in Eqns. (13) - (15). Firstly, Eqns. (10) - (12) are transformed into an *initial value problem:*

$$F' = \mathcal{F}_1, \mathcal{F}_1' = \mathcal{F}_2, \mathcal{F}_1' = -F\mathcal{F}_2 + \frac{2m}{m+1}F_1^2 + \frac{A_5}{A_2}M\mathcal{F}_1 + \frac{k}{A_2}\mathcal{F}_1 -$$
$$\frac{2}{m+1}\frac{A_4}{A_2}R_i(\theta + \eta\Phi) ,$$
(18)

$$\theta' = \mathcal{G}_1, \mathcal{G}_1' = \frac{-F\mathcal{G}_1 + \dfrac{2(2m-1)}{m+1}\mathcal{F}_1\theta + D_u\mathcal{H}_1'}{\dfrac{A_6}{A_3 P_r} + \dfrac{4R_d}{3A_3}},$$
(19)

$$\Phi' = \mathcal{H}_1, \mathcal{H}_1' = -S_c F\mathcal{G}_1 + \frac{2S_c(2m-1)}{m+1}\mathcal{F}_1\Phi + S_c S_r \mathcal{G}_1'.$$
(20)

The associated boundary conditions now take the form:

$$u = \mathcal{S}, \mathcal{H}_1 = \mathcal{S}_3 \mathcal{F}_1 = 1 + \xi\mathcal{F}_1', \mathcal{F}_1' = \mathcal{S}_1, \mathcal{G}_1 = \mathcal{S}_2, \theta = 1, \Phi = 1 \text{ at } y = 0. \quad (21)$$

An appropriate initial value is elected for $\mathcal{S}_1, \mathcal{S}_2$ and $\mathcal{S}_3$. The step size is selected $\Delta y = 0.0001$. Numerical computations are executed in MATLAB symbolic software [34, 45].

4. VALIDATION WITH EARLIER STUDIES

To verify the accuracy of the MATLAB shooting quadrature computations, comparisons with previous studies have been conducted. **Table 1** shows the thermophysical properties of base fluid and nanoparticles (Fe_3O_4).

Table 1: Thermophysical properties of nanoparticles and base fluid.

Property	Water	Fe$_3$O$_4$
$\rho\left(\dfrac{kg}{m^3}\right)$	997.1	5200
$K\left(\dfrac{W}{mkel}\right)$	0.613	80.6
$C\left(\dfrac{J}{kgKel}\right)$	4179	670
$\beta\left(\dfrac{1}{Kel}\right) \times 10^{-6}$	210	13
$\sigma\left(\dfrac{S}{m}\right)$	0.05	25000

Table 2 and Table 3 document the numerical comparisons of skin friction i.e. $F''(0)$ and Nusselt number i.e. $-\theta'(0)$ for multiple values of power-law stretching parameter (m) and Prandtl number P_r with the previously published data [35-39] by considering $k = M = R_d = D_u = S = R_i = \phi = \beta = 0$. From these tables, it is evident that the shooting results are in excellent agreement with the previously published results. Confidence in the shooting quadrature is therefore justifiably high.

Table 2: Comparison of skin friction coefficient $-F''(0)$ with the published results for $k = M = S = R_i = \phi = \beta = 0$.

m	Shooting Solution	GDQ Solution	Hammad and Ferdows [35]	Cortell [36]
0	0.6276	0.6268	0.6369	0.6276
3	1.1486	1.1483	1.1481	1.1486
10	1.2349	1.2348	1.2349	1.2342
20	1.2574	1.2573	1.2574	1.2574

Table 3: Comparison of Nusselt number function, $-\theta'(0)$, with the published results for $k = R_d = D_u = \beta = M = S = R_i = 0$.

P_r	Shooting Solution	GDQ Solution	Ali *et al.* [37]	Yih [38]	Aurangzaib *et al.* [39]
0.72	0.8086	0.8086	0.8086	0.8086	0.8086
3	1.9237	1.9236	1.9237	1.9237	1.9237
10	3.7207	3.7206	3.7208	3.7207	3.7207

It is of further note that with increasing power-law stretching parameter (Table 2) there is a marked

elevation in skin friction i.e. the magnetic nanofluid boundary layer flow is decelerated with an increase in sheet stretching velocity. Momentum is extracted from the boundary layer flow and the implication is that significant modification (regulation) in momentum characteristics at the wall is achieved with progressive enhancement in the sheet stretching velocity ($m = 3, 10, 20$) compared to when stretching is absent ($m = 0$). With higher Prandtl number (Table 3), there is a progressive elevation also in Nusselt number. This indicates that as thermal diffusivity decreases relative to momentum diffusivity of the nanofluid, the migration of heat to the wall (sheet) is encouraged. This will also result in a decrease in temperatures in the nanofluid and a thinning in thermal boundary layer thickness i.e. the bulk nanofluid flow will be cooled achieving the desired objective of regulating temperature distribution during manufacturing, as noted by Viskanta [44].

5. FURTHER VALIDATION WITH GDQ CODE

Further corroboration of the shooting solutions is achieved with a different computational technique. This serves to add a dual confidence in the computations. The fundamental premise of generalized differential quadrature (GDQ) is that the differentiation of a function with respect to a variable of space on a given set of points is approximated as a *weighted linear sum* at the selected points in the domain of that variable. The GDQ approach was pioneered in fluid mechanics and engineering dynamics applications by Shu *et al.* [40] to improve the Bellman differential quadrature (DQM) method which is based on integral quadrature and was introduced much earlier in 1972. It generally approximates the differentiation of function with respect to space variables at a sample grid point as a weighted linear summation of all the values of function at all grid points in the domain. The basic idea for computing the weighting coefficients by GDQ is based on the analysis of a high order polynomial approximation and linear vector space. The weighting coefficients of the first order derivative are calculated by a simple algebraic formulation, and the weighting coefficients of the second and higher order derivatives are given by a recurrence relationship. The GDQ approach is equivalent to the highest order finite difference scheme. This method is also described in some detail in the context of nanofluid dynamics by Bég [46] and also magnetohydrodynamics by Bég [47]. To illustrate the approximation in the GDQ, let us consider a function, $f(\eta)$ defined in the domain $0 < \eta \le a$. According to the GDQ, the function $f(\eta)$ can be approximated as follows:

$$\frac{\partial^r f(\eta)}{\partial \eta^r}\bigg|_{\eta,\tau=\eta_i} = \sum_{m=1}^{N_\eta} A_{im}^{(r)} f(\eta_m) = \sum_{m=1}^{N_\eta} A_{ij}^{(r)} f_m, \quad i = 1, 2, \dots, N_\eta. \tag{22}$$

Therefore, the first-order derivatives have following weighting coefficients in the direction of η_i is given by the formula [46, 47]:

$$A_{ij} = \begin{cases} -\sum_{j=1,\ i\neq j}^{N_\eta} A_{ij}, & i = j, \\ \dfrac{1}{a}\dfrac{M(\eta_i)}{(\eta_i - \eta_j)M(\eta_j)}, & i \neq j, \end{cases} \quad i,j = 1,2,\dots,N_\eta, \quad M(\eta_i) = \prod_{j=1,\ i\neq j}^{N_\eta} (\eta_i - \eta_j) \tag{23}$$

The weighting coefficients of the higher-order derivative can be obtained as follows:

$$\left[A_{ij}^{(r)}\right] = \left[A_{ij}^{(r-1)}\right]\left[A_{ij}\right] = \left[A_{ij}\right]\left[A_{ij}^{(r-1)}\right]. \tag{24}$$

It is pertinent to deploy Chebyshev-Gauss-Lobatto grid distribution:

$$\frac{\eta_i}{a} = \frac{1}{2}\left[1 - \cos\left(\frac{i-1}{N_\eta - 1}\pi\right)\right] \qquad\qquad i = 1, 2, \dots, N_\eta, \tag{25}$$

According to the GDQ, the discretized governing equations and the appropriate boundary conditions can then be generated, although for brevity we have omitted these lengthy algebraic expressions here. In the emerging formulations, parameters arise, which represent the second- and third-order weighting coefficients, respectively. The values of the similarity flow variables i.e. F_i, θ_i, Φ_i at each node in the solution domain can be obtained. These may then in turn be utilized to compute the wall functions i.e. skin friction, Nusselt number, Sherwood number. Comparisons of the Shooting quadrature solutions and the GDQ code (which is executed on an SGI Octane desk workstation and takes approximately forty seconds to converge) for skin friction coefficient, Nusselt number, Sherwood number, are presented in Table 2 and 3 (for the simpler cases from the literature). Excellent correlation is achieved. Confidence in the present shooting quadrature MATLAB solutions is therefore justifiably very high.

6. RESULTS AND DISCUSSION

Symbolic computational software, MATLAB has been utilized to analyze the effects of selected parameters on the magnetic nanofluid transport characteristics i.e. Hartmann number *M*,

porosity parameter k, slip parameter ξ, Richardson number R_i, concentration to thermal buoyancy ratio η, radiation parameter R_d, Prandtl number Pr, Soret number S_r, Dufour parameter D_u and Schmidt number S_c respectively. Table 4 shows the influence of some of these parameters on skin friction (C_F), Nusselt number (Nu_r) and Sherwood number (Sh_r). Graphical plots for the evolution of velocity, temperature and nano-particle concentration functions versus transverse coordinate (ζ) are illustrated in **Figs. 2 to 11**. Water is assumed as the base fluid in all computations ($Pr = 6.2$). Table 4 indicates that with increasing Hartmann number (M) there is a strong elevation in skin friction at the boundary (sheet surface). Similarly, with increasing Darcian parameter (k) the skin friction is elevated since permeability. Increasing Prandtl number (Pr) weakly increases skin friction, strongly enhances Nusselt number but reduces the Sherwood number. With increasing radiation parameter (Rd) the skin friction is marginally reduced whereas the Nusselt number is significantly altered and the Sherwood number is slightly decreased. Thermal radiative flux therefore exerts a marked influence on transport characteristics at the wall. An elevation in Dufour number depresses both skin friction and Nusselt number but serves to strongly increase the Sherwood number since the Dufour effect is associated primarily with a concentration gradient. This enhances nano-particle diffusion to the wall from the bulk nanofluid but simultaneously decreases thermal diffusion to the wall i.e. cools the boundary. With increasing Soret number, the thermal gradient is influenced and indirectly modifies the concentration diffusion of nano-particles. Skin friction is reduced as is Sherwood number, whereas the Nusselt number is elevated. Since heat and mass transfer (thermal and species diffusion) occur simultaneously in the moving magnetic nanofluid, the cross-diffusion effects of Soret and Dufour diffusion result in complex relationships between the fluxes and the driving potentials. An energy flux is generated not only by temperature gradients, but also by nano-particle species concentration gradients also. The energy flux caused by a composition gradient is the Dufour or diffusion-thermo effect whereas the mass (species) flux mobilized by temperature gradients is the Soret or thermal-diffusion effect. Since both energy and nano-particle species conservation equations feature terms from the other equations e.g. $+D_u\Phi''$ arises in the energy eqn. (11) and $-S_C S_r \theta''$ arises in the nano-particle species eqn. (12) there is a "cross-diffusion" and intimate interplay between the two diffusion effects which clearly influences sheet stretching transport characteristics. These effects have also been lucidly highlighted by Viskanta and Bergman [48] who have computed similar patterns of behavior as observed in Table 4. They have further emphasized that such effects are amplified

when density differences arise as characterized by dual thermal and species buoyancy forces, both of which are incorporated in the present simulations. It is of further note that Table 4 provides a solid benchmark for other researchers to extend the current model and to compare alternative numerical methods with the present shooting and GDQ techniques. Table 4 further implies that with increasing Schmidt number there is a marginal increase in skin friction and weak depression in Nusselt number whereas there is a very strong enhancement in Sherwood number. Mass diffusion of nano-particles to the wall is therefore the primary effect achieved by elevating the momentum diffusion rate relative to the species (nano-particle) diffusion rate (Schmidt number relates these two diffusion rates).

Fig. (2) to Fig. (6) display the variation of velocity profile for different values of slip parameter β, Hartmann number M, Darcy parameter k, Richardson number R_i, and concentration buoyancy ratio η, respectively. It can be observed from Fig. (2) that increasing magnetic field i.e. (greater Hartmann number M) opposes the boundary layer flow. The Lorentz force is a magnetic drag force which acts transverse to the applied magnetic field i.e. along the sheet extrusion direction. It arises in the term, $-\frac{A_5}{A_2}M^2F'$ in the momentum conservation Eqn. (10). This negative body force decelerates the boundary layer flow and opposes momentum diffusion as observed in Fig. (2). When $M = 1$ the Lorentz force and viscous hydrodynamic force in the magnetic nanofluid regime are equivalent. This results in maximum velocity magnitudes and a thin momentum boundary layer. However, as M exceeds unity, the momentum boundary layer is progressively thickened due to flow retardation. Similar findings have been reported by Hakeem *et al*. [22], Zeeshan *et al*. [29] and Haq *et al*. [31], although they neglected cross-diffusion effects in their simulations. In magnetic nano-materials processing the significant flow control achieved with strategic selection of magnetic field strength enables engineers to modify the internal constitution of nano-polymers and this has also been emphasized by Müller [12]. From Fig. (3) it is evident that the Darcy drag parameter (k) also induces a deceleration in the flow. The Darcian drag term in the transformed momentum eqn. (10) i.e. $-\frac{k}{A_2}F'$, is a *linear impedance term*, which is *inversely proportional to the actual permeability of the medium*. Even with sparse packing of the medium, the Darcian force retards the momentum development (greater k values imply lower permeability and an increase in density of solid matrix fibers in the regime). Since the analysis is restricted to low Reynolds numbers, viscous effects will dominate and inertial drag is negligible. As with

magnetic field effect (Fig 2), the prominent modifications in velocity are observed at intermediate distances from the sheet surface (wall). Asmptotically, smooth profiles are computed in the free stream indicating that a sufficiently large infinity boundary condition has been prescribed in the shooting quadrature program. The impact of both magnetic field and porous medium fibers is non-trivial and demonstrates that both mechanisms are effective in controlling the flow. Backflow is however never induced and velocities remain positive throughout the regime indicating that boundary layer flow separation or reversal never arises. The regime is therefore controlled and laminar in nature. Fig. (4) shows the impact of wall hydrodynamic slip parameter, β, on velocity profiles. It is evident that with greater slip there is a progressive depletion in velocity magnitudes. The non-adherence of the nanofluid to the wall, implies that momentum diffusion is inhibited in this vicinity. There is a phase lag between the wall characteristics and the bulk nanofluid flow and the stretching sheet velocity is reduced. Although only first order (linear) slip is analyzed, the effect is distinctly maximized at the wall (where the slip arises) and gradually decays into the boundary layer transverse to the wall. This is corroborated by several other investigations including Mabood *et al.* [14] and Nandy and Mahaparta [18]. An important deduction is that when hydrodynamic slip is neglected, velocity magnitudes are clearly over-predicted. Thus, to achieve more realistic estimates of the stretching sheet dynamics, engineers are recommended to incorporate slip effects in mathematical models. Fig. (5) reveals the response of velocity distributions to an increase in Richardson number, R_i. This parameter features in the positive thermal buoyancy body force term in Eqn. (10) i.e. $+\frac{2A_4}{(m+1)A_2}R_i(\theta + \eta\Phi)$. It also couples the temperature field (θ) and nano-particle concentration field (Φ). With elevation in Richardson number, the thermal buoyancy force is enhanced. This aids momentum diffusion and leads to an acceleration in the flow i.e. boost in velocity magnitudes and this effect penetrates a much wider range of the boundary layer. The boost in kinetic energy in the flow is therefore maximum when $Ri =4$ and minimal when $Ri = 1$ (thermal buoyancy and viscous hydrodynamic force are equal). The damping effect of viscosity in the nanofluid is therefore successfully overcome with thermal buoyancy. It is also noteworthy that when $Ri = 0$ the regime morphs to *forced convection* since thermal (and species) buoyancy effects are de-coupled from the velocity field. Fig. (6) shows the influence of concentration to thermal buoyancy ratio, η on velocity profiles.

M	k	P_r	R_d	D_u	S_r	S_c	C_F	Nu_r	Sh_r
2	0.5	6.2	1	0.2	1	1	3.7688		
3							4.1007		
4							4.3789		
	0.6						3.7960		
	1						3.9008		
	1.5						4.0235		
		3					4.0140	2.9497	0.9559
		6					4.0232	3.2695	0.9529
		10					4.0273	3.4229	0.9515
			1.5				4	3.2108	0.9609
			2				3.9853	3.2492	0.9662
			3				3.9682	3.4531	0.9728
				0.05			4.0296	3.4958	0.9507
				0.1			4.0276	3.4243	0.9514
				0.2			4.0235	3.2812	0.9528
					0.5		4.0428	3.1669	1.1952
					0.9		4.0268	3.2626	0.9915
					1.5		4.0102	3.3540	0.8045
						0.3	3.9845	3.4851	0.55
						0.6	4.0067	3.3728	0.7672
						1.0	4.0201	3.3	0.9139

Table 4: Numerical results of Nusselt number, Sherwood number and skin friction coefficient for multiple values of $M, P_r, Rd, \ k, D_u, S_c$ and S_r. (Other parameters are fixed).

Again, this parameter features in the momentum eqn. (10); however, it connects both species (nano-particle concentration) and thermal buoyancy forces, whereas the Richardson number is confined to the purely thermal buoyancy (natural convection) effect. The parameter $\eta = \frac{A_6(\rho\beta_{\tilde{C}})_{nf}}{A_4(\rho\beta_{\tilde{T}})_{nf}}\left(\frac{\tilde{C}_w - \tilde{C}_\infty}{\tilde{T}_w - \tilde{T}_\infty}\right)$ and it allows the sensitivity of both buoyancy forces to be addressed. For $\eta = 1$ both thermal and nanoparticle species buoyancy force assume equal magnitudes. When $\eta < 1$, thermal buoyancy dominates whereas when $\eta > 1$, the nano-particle species buoyancy dominates. There is progressive acceleration in the nanofluid flow with increasing buoyancy ratio and this pattern s sustained for a large range of the transverse coordinate, ζ. This is probably attributable

to the thermal and species diffusion occurring throughout the boundary layer, as noted by Viskanta and Bergman [48], Gebhart *et al*. [49] and Magyari and Postelnicu [50], among others.
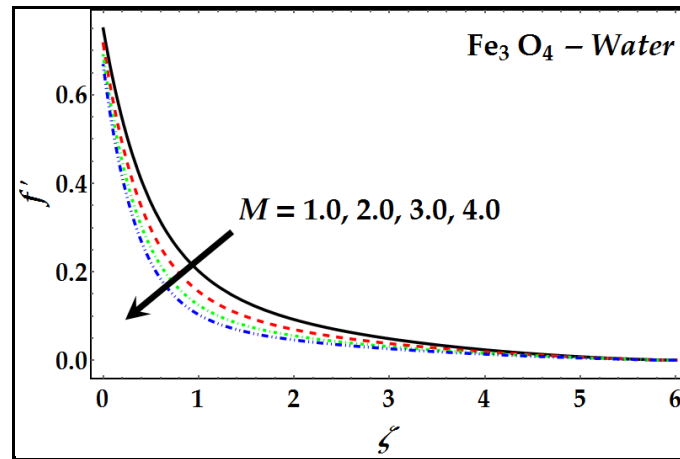

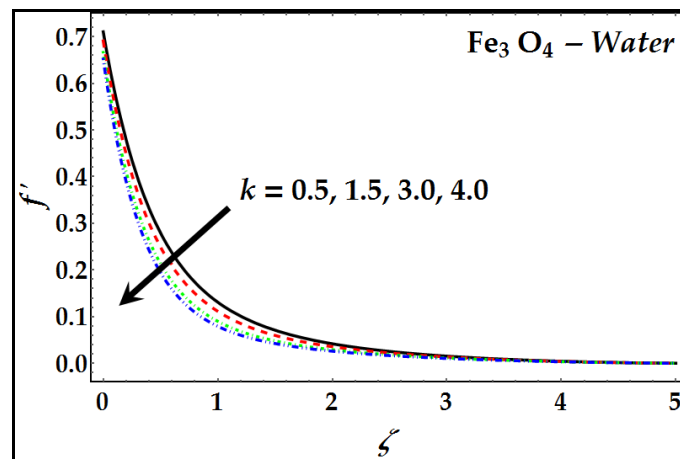**Fig. 2.** Distribution of velocity against multiple values of M.

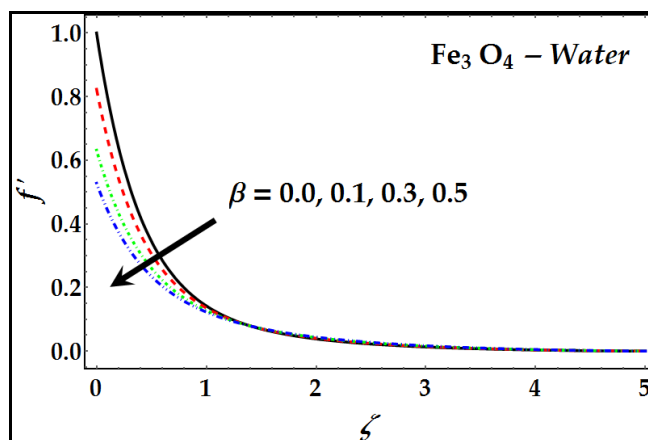**Fig. 3.** Distribution of velocity against multiple values of k.

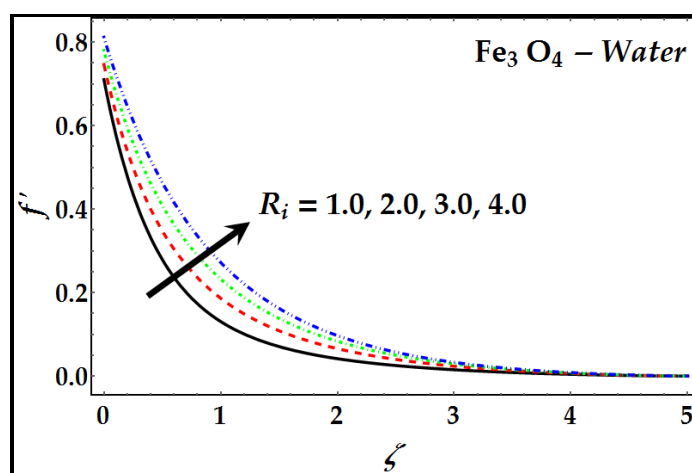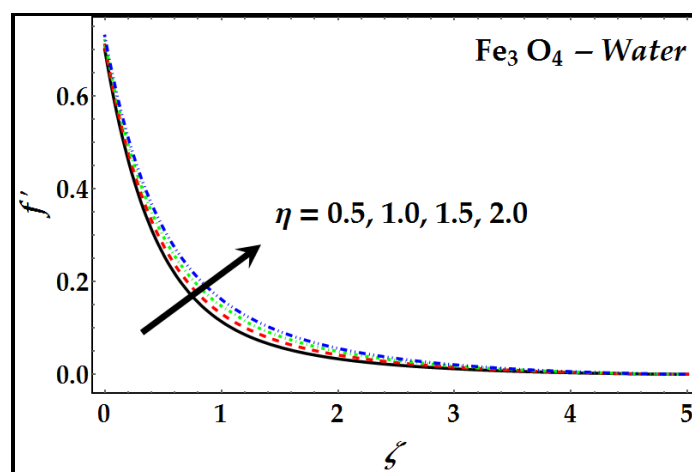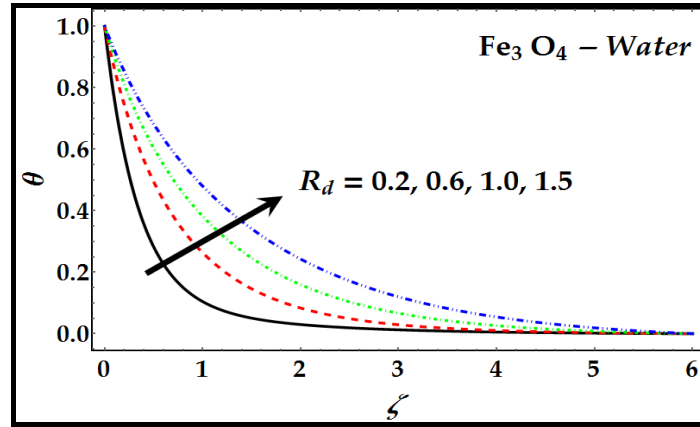**Fig. 4.** Distribution of velocity against multiple values of β.

Fig. 5. Distribution of velocity against multiple values of R_i.

Fig. 6. Distribution of velocity against multiple values of η.

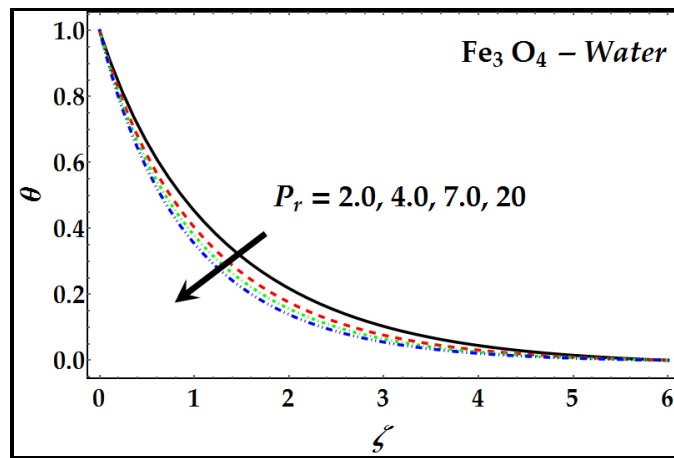**Fig. 7.** Distribution of temperature against multiple values of R_d.

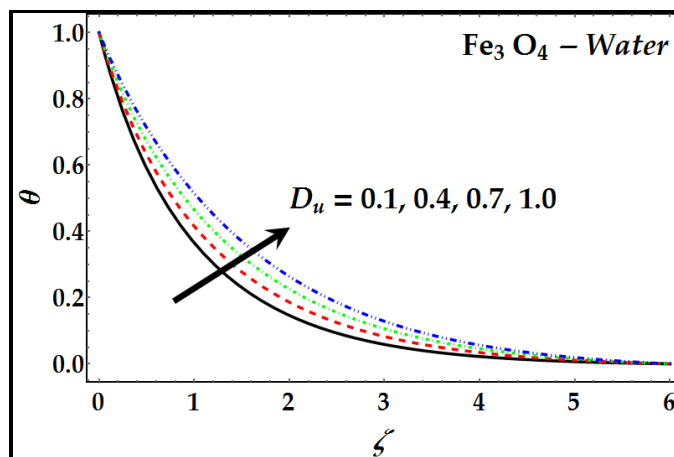**Fig. 8.** Distribution of temperature against multiple values of P_r.

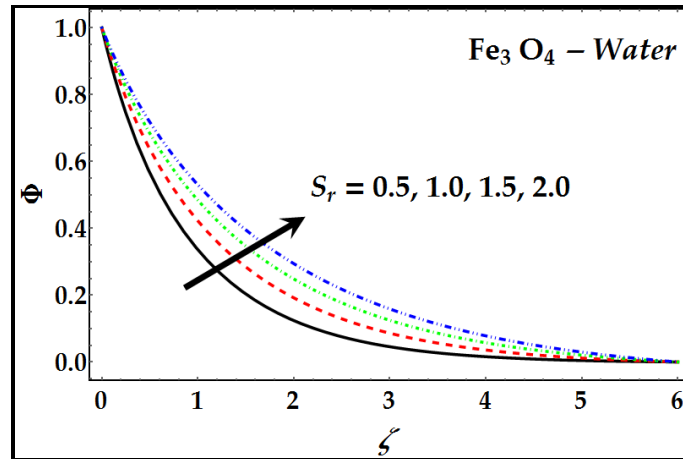**Fig. 9.** Distribution of temperature against multiple values of D_u.

Fig. 10. Distribution of nanoparticle concentration against multiple values of S_r.
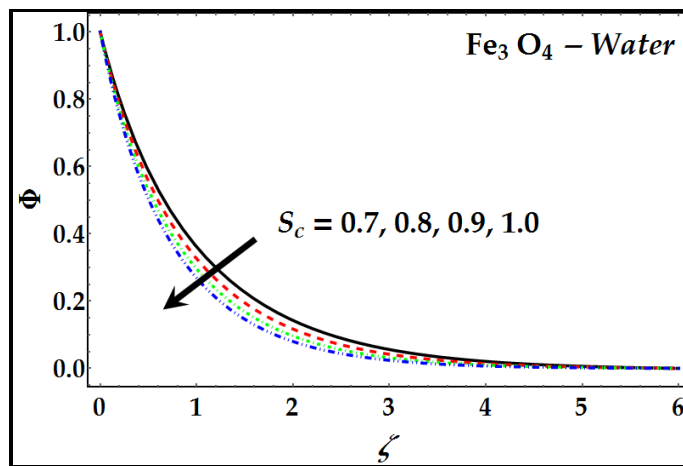

Fig. 11. Distribution of nanoparticle concentration against multiple values of S_c.

Fig. (7)-(9) show the evolution in temperature distribution for multiple values of Dufour parameter D_u, radiation parameter R_d, and Prandtl number P_r. It can be observed from Fig. (7) that increasing radiation parameter R_d, significantly enhances temperature magnitudes. This parameter appears in the energy conservation eqn. (11), in the term, $+\frac{4R_d}{3A_3}\theta''$. This augments the basic thermal diffusion term, $\frac{A_6}{A_3 P_r}\theta''$, which characterizes purely conductive-convective transport, based on the Fourier conduction law. The presence of radiative heat flux energizes the magnetic nanoliquid regime and prominently elevates temperatures since supplementary heat is added to the nanoliquid. Thermal boundary layer thickness is therefore also enhanced in the regime. Even a slight modification in radiative parameter exerts a marked influence on heat transfer characteristics

across the boundary layer transverse to the stretching sheet wall. In the absence of thermal radiation, $R_d \rightarrow 0$. As noted by Viskanta [44], the neglection of radiative effects in high temperature materials processing therefore severely under-predicts actual temperatures in the extruded material. This will also lead to erroneous results in Nusselt number (wall heat transfer gradient) computation and will incorrectly predict thermal fields. The current results are in agreement with Viskanta's computations and indeed also concur with other major studies of radiative nanofluid dynamics, including Abbas *et al.* [16], Hakeem *et al.* [22] and Haq *et al.* [31]. The Rosseland diffusion flux model therefore, while simple and restricted to optically-dense media (magnetic nanofluids) does successfully capture general radiative heat transfer effects in materials processing systems. This provides a good platform for extension of the current model to more sophisticated radiative flux models such as the STS (surface to surface) model and P1 differential flux model, both of which have also been considered in recent simulations by Kuharat *et al.* [51], albeit for solar collector internal nanofluid dynamics. Fig. (8) illustrates that an increase in Prandtl number Pr leads to a strong reduction in temperature distribution. Prandtl number is inversely proportional to effective thermal conductivity of the magnetic nanofluid. $Pr = 2$ corresponds to dense gases and $Pr = 7$ approximates aqueous base fluids. $Pr = 20$ is associated with low density polymeric solutions. As Pr is increased, thermal conductivity of the nanofluid is decreased. The heat transported by molecular conduction is therefore suppressed which manifests in a decrease in temperatures and a depletion in thermal boundary layer thickness. Cooling of the stretching sheet regime is therefore achieved with higher Prandtl number whereas heating is observed with lower Prandtl numbers. Prandtl number also relates the momentum diffusion rate and the thermal diffusion rate. As Prandtl number increases (beyond unity) the momentum diffusion rate greatly exceeds thermal diffusion rate which results in a suppression of thermal diffusion and lower temperatures. Fig. (9) is displayed for multiple values of Dufour parameter D_u. The Dufour effect, as noted earlier, describes the heat flux due to the nano-particle mass concentration gradient and is characteristic of high-density variation scenarios of the irreversible type e.g. magnetic nanofluid viscous flows. With increasing Dufour number, the concentration gradient progressively contributes greater thermal energy to the regime. This elevates temperatures significantly across the boundary layer and also boosts thermal boundary layer thickness. As noted by Viskanta [44], neglection of the Dufour effect will therefore substantially under-predict actual temperatures in materials processing simulations. Fig. (10) and Fig. (11) are drawn for concentration distribution

against multiple values of Soret number S_r and Schmidt number S_c. Fig. (10) shows that the nano-particle concentration distribution and the associated species boundary layer thickness increase for large values of Soret number S_r. The Soret i.e. thermo-diffusion effect, quantifies the contribution of thermal gradient to nano-particle species diffusion. It is the reverse mechanism to the Dufour effect. Both effects are beneficial to the thermal and species diffusion respectively and are useful therefore in the manipulation of nanomaterials constitution in materials processing since they permit more homogenous heat and nano-particle doping to be achieved in for example nano-coating manufacturing. This leads to improved quality in coating synthesis and inevitably enhanced performance in applications. Finally, Fig. (11) visualizes the impact of Schmidt number S_c on nao-particle concentration profile. Schmidt number embodies the ratio between momentum and mass diffusivity. It is evident that increasing Schmidt number tends to reduce the concentration magnitudes markedly and this depression extends for a considerable region in the boundary layer. When $Sc < 1$ the momentum diffusion rate is exceeded by the nano-particle species diffusion rate and maximum concentration magnitudes are computed. Conversely when $Sc > 1$ the momentum diffusion rate exceeds the species diffusion rate and this manifests in a depletion in concentration values. For the case of $Sc = 1$ both momentum and nano-particle species diffusion rates are equivalent as are the boundary layer thicknesses. The nature of the nano-particle (iron oxide) suspended in water is therefore critical to controlling species diffusion rates in materials processing operations. It is finally to be noted that Fickian diffusion has been assumed in the current simulations. Future investigations could explore non-Fickian models [52] which may furnish further insight into molecular diffusion in nano-coating sheet dynamics.

7. CONCLUSIONS

In this article, motivated by simulating smart nanomaterial fabrication processes, a comprehensive mathematical model has been developed for the radiative magnetohydrodynamic boundary layer slip flow of Fe_3O_4 -water magnetite nanofluid from a vertical non-linear porous stretching sheet. Soret and Dufour cross-diffusion effects have been included in the model. Thermal and species concentration buoyancy effects have also been incorporated and the Rosseland diffusion flux algebraic approximation has been utilized. Via appropriate similarity variables, the partial differential boundary value problem has been transformed into an ordinary differential boundary value problem which is solved numerically using a shooting technique in

MATLAB symbolic software. Validation with earlier published studies is included. Further verification of the shooting solutions with a generalized differential quadrature (GDQ) code is also conducted. The principal findings of the simulations are summarized below:

- Velocity is strongly damped with increasing Hartmann number (magnetic body force) effect and Darcian drag effect (i.e. decreasing permeability of the medium).

- Increasing hydrodynamic wall slip induces a substantial depletion in nanofluid velocity magnitudes.

- Increasing radiative flux and Dufour (diffuso-thermal) effect strongly energize the boundary layer and enhance the temperature magnitudes (and thermal boundary layer thickness) very significantly.

- Increasing Soret number (thermo-diffusion) enhances the nano-particle concentration values (and nano-species boundary layer thickness) whereas increasing Schmidt number induces the reverse effects.

- Increasing Richardson number and thermal/species buoyancy ratio parameter substantially accelerate the magnetic nanofluid flow and simultaneously reduce the momentum (hydrodynamic) boundary layer thickness.

- An elevation in Dufour number reduces both skin friction (dimensionless wall shear stress) and Nusselt number (dimensionless wall heat transfer gradient) whereas it dramatically elevates the Sherwood number (wall nano-particle species gradient).

- With increasing Soret number, skin friction and Sherwood number are both depleted whereas the Nusselt number is boosted.

- The present nanofluid model reduces to a simple Newtonian fluid (nanoscale effects neglected) by taking nano-particle volume fraction, $\phi = 0$.

- Both MATLAB shooting quadrature and GDQ computation provide excellent numerical strategies for simulating nonlinear magnetic nanofluid fabrication processes.

The current investigation has provided some good insight in ferrofluid (magnetic nanofluid) synthesis processes employed in industrial manufacturing. However, it has neglected *non-Fickian diffusion* and *non-Fourier thermal relaxation physics* [52] and furthermore has ignored *rheological (non-Newtonian)* aspects [53]. These constitute important extensions to the current simulations and are being addressed presently. Additionally, the mathematical and numerical approaches

adopted in the current work may be logically applied to studying hybrid copper-silver-water nanofluids [54] and possibly in analyzing laser-pulse heating of deformable porous media [55].

REFERENCES

[1] M. Arai and T. Suidzu, Porous ceramic coating for transpiration cooling of gas turbine blade, *Journal of Thermal Spray Technology,* 22, 690–698 (2013).

[2] S.U.S. Choi, Nanofluids: from vision to reality through research (*Micro/Nanoscale Heat Transfer—Part I*), *ASME J. Heat Transfer,* 131(3), 033106 (2009).

[3] J. Texter *et al.*, Nanofluid acrylate composite resins—initial preparation and characterization, *Polym. Chem.*, 2, 1778-1788 (2011)

[4] O. Anwar Bég, S. Kuharat, R. Mehmood, Rabil Tabassum and M. Babaie, Oblique radiative solar nano-polymer gel coating heat transfer and slip flow: manufacturing simulation, *ICHTFM 2018: 20th International Conference on Heat Transfer and Fluid Mechanics, Istanbul, Turkey, August 16 – 17* (2018).

[5] S. Bhageli *et al.,* Synthesis and experimental investigation of the electrical conductivity of water-based magnetite nanofluids, *Powder Technology*, 274, 426-430 (2015).

[6] I.Nkurikiyimfura *et al.,* Heat transfer enhancement by magnetic nanofluids—A review, *Renewable and Sustainable Energy Reviews*, 21, 548-561 (2013).

[7] M. Bahiraei and M. Hangi, Flow and heat transfer characteristics of magnetic nanofluids: A review, *J. Magnetism and Magnetic Materials*, 374, 125-138 (2015).

[8] N. G. Jia *et al.,* Ferrofluids for heat transfer enhancement under an external magnetic field, *International Journal of Heat and Mass Transfer*, 123, 110-121 (2018).

[9] O. Anwar Bég, Ayesha Sohail, T.A. Bég and A. Kadir, B-spline collocation simulation of nonlinear transient magnetic nano-bio-tribological squeeze film flow, *J. Mechanics in Medicine and Biology,* 18, 1850007.1- 1850007.20 (20 pages) (2018).

[10] B.C. Sakiadis, Boundary layer behaviour on continuous solid flat surfaces, *J. Amer. I. ChemE*, 7, 26-28 (1961).

[11] L. Crane, Flow past a stretching plate, *Z. Angew. Math. Phys.,* 21, 645-647 (1970).

[12] K. Müller *et al.,* Review on the processing and properties of polymer nanocomposites and nanocoatings and their applications in the packaging, automotive and solar energy fields, *Nanomaterials, 7*(4), 74-90 (2017).

[13] P. Guo *et al*., Nanomaterial preparation by extrusion through nanoporous membranes, *Small* 2018, 1703493.1-16 (2018).

[14] F. Mabood, W.A. Khan, A.I.M. Ismail, MHD boundary layer flow and heat transfer of nanofluids over a nonlinear stretching sheet: a numerical study, *J. Magn. Mag. Mater*., 374, 569-576 (2015).

[15] 0. Anwar Bég, M.S. Khan, I. Karim, M.M. Alam and M. Ferdows, Explicit numerical study of unsteady hydromagnetic mixed convective nanofluid flow from an exponentially stretching sheet in porous media, *Applied Nanoscience,* 4 (8) 943-957 (2014).

[16] Z.Abbas, M. Naveed and M. Sajid, Hydromagnetic slip flow of nanofluid over a curved stretching surface with heat generation and thermal radiation, *J. Molecular Liquids*, 215, 756-762 (2016).

[17] T. Thumma, O. Anwar Bég and A. Kadir, Numerical study of heat source/sink effects on dissipative magnetic nanofluid flow from a non-linear inclined stretching/shrinking sheet, *J. Molecular Liquids,* 232, 159-173 (2017).

[18] S.K. Nandy, T.R. Mahaparta, Effects of slip and heat generation/absorption on MHD stagnation point flow of nanofluid past a stretching/shrinking surface with convective boundary conditions, *Int. J. Heat Mass Transf*., 64, 1091-1100 (2013).

[19] Ayub M, Abbas T, Bhatti MM. Inspiration of slip effects on electro-magneto-hydrodynamics (EMHD) nanofluid flow through a horizontal Riga plate, *Europ Phys J Plus*, 131: 1-9 (2016).

[20] M.J. Uddin, O. Anwar Bég and N.S. Amin, Hydromagnetic transport phenomena from a stretching or shrinking nonlinear nanomaterial sheet with Navier slip and convective heating: a model for bio-nano-materials processing, *J. Magnetism Magnetic Materials,* 368, 252-261(2014).

[21] N. Shukla, P. Rana, O. Anwar Bég, Bani Singh and A. Kadir, Homotopy study of magnetohydrodynamic mixed convection nanofluid multiple slip flow and heat transfer from a vertical cylinder with entropy generation, *Propulsion and Power Research (2019). https://doi.org/10.1016/j.jppr.2019.01.005 (16 pages)*

[22] Hakeem AA, Ganesh NV, Ganga B. Magnetic field effect on second order slip flow of nanofluid over a stretching/shrinking sheet with thermal radiation effect. *J. Magnetism Magnetic Materials,* 381, 243-257 (2015).

[23] N.A. Amirsom, M.F.M. Basir, M. J. Uddin, A. I. Ismail, O. Anwar Bég and Ali Kadir, Computation of melting dissipative magnetohydrodynamic nanofluid bioconvection with second order slip and variable thermophysical properties, *Applied Sciences (Applied Biosciences and Bioengineering section),* 9, 1-22 (2019).

[24] Alkahtani B, Abel MS, Aly EH. Magnetohydrodynamic steady boundary layer stagnation point of nanofluid flow with heat and mass transfer over a stretching sheet with full slip effects. *J Comput Theor. Nanosci.,* 12, 5379-5385 (2015).

[25] M. J. Uddin, M.N. Kabir, O. Anwar Bég and Y. Alginahi, Chebyshev collocation computation of magneto-bioconvection nanofluid flow over a wedge with multiple slips and magnetic induction, *Proc. IMechE: Part N-Journal of Nanomaterials, Nanoengineering and Nanosystems (2018). DOI: 10.1177/2397791418809795 (15 pages)*

[26] Z. Said *et al.,* Radiative properties of nanofluids, *Int Comm Heat And Mass Transfer*, 46, 74-84 (2013).

[27] P.D. Shima *et al.,* Synthesis of aqueous and nonaqueous iron oxide nanofluids and study of temperature dependence on thermal conductivity and viscosity, *J. Phys. Chem. C*, *114* (44), 18825–18833 (2010).

[28] Bhatti MM, Abbas T, Rashidi MM, Ali MES. Numerical simulation of entropy generation with thermal radiation on MHD Carreau nanofluid towards a shrinking sheet. *Entropy,* 18: 200 (2016).

[29] Zeeshan A, Majeed A, Ellahi R. Effect of magnetic dipole on viscous ferro-fluid past a stretching surface with thermal radiation. *J Molecular Liquids,* 215: 549-554 (2016).

[30] Bhatti MM, Rashidi MM. Entropy generation with nonlinear thermal radiation in MHD boundary layer flow over a permeable shrinking/stretching sheet: numerical solution. *J Nanofluids,* 5:543-548 (2016).

[31] Haq RU, Nadeem S, Khan ZH, Akbar NS. Thermal radiation and slip effects on MHD stagnation point flow of nanofluid over a stretching sheet. *Physica E,* 65: 17-23 (2015).

[32] J. Prakash, E.P. Siva, D Tripathi, S. Kuharat and O. Anwar Bég, Peristaltic pumping of magnetic nanofluids with thermal radiation and temperature-dependent viscosity effects:

modelling a solar magneto-biomimetic nanopump, Renewable Energy (2018). 18 pages. doi.org/10.1016/j.renene.2018.08.096 0960-1481

[33] Bhatti MM, Rashidi MM. Effects of thermo-diffusion and thermal radiation on Williamson nanofluid over a porous shrinking/stretching sheet. *J Molecular Liquids,* 221: 567-573 (2016).

[34] A. Quarteroni and F. Saleri, *Scientific Computing with MATLAB and Octave*. Springer, New York (2006).

[35] Hamad MAAA, Ferdows M. Similarity solutions to viscous flow and heat transfer of nanofluid over nonlinearly stretching sheet. *Appl Math Mech Eng*., 33:923–930 (2012).

[36] Cortell R. Viscous flow and heat transfer over a nonlinearly stretching sheet. *Appl Math Computation,* 184: 864–873 (2007).

[37] Ali FM, Nazar R, Arifin NM, Pop I. Effect of hall current on MHD mixed convection boundary layer flow over a stretched vertical flat plate. *Meccanica,* 46: 1103–1112 (2011).

[38] Yih KA. Free convection effect on MHD coupled heat and mass transfer of a moving permeable vertical surface. *Int Commum Heat Mass Transfer,* 29: 95–104 (1999).

[39] Aurangzaib A, Kasim RM, Mohammad NF, Shafie S. Effects of thermal stratification on MHD free convection with heat and mass transfer over an unsteady stretching surface, Hall current and chemical reaction. *Int J Adv Eng Sci Appl Math,* 4: 217–225 (2012).

[40] Shu, C., Chew, Y. T. and Richards, B. E., Generalized differential-integral quadrature and their application to solve boundary layer equations, *International Journal* for *Numerical Methods* in *Fluids*, 21, 723– 733 (1995).

[41] O. Anwar Bég, Bakier, A.Y. and V.R. Prasad, Numerical study of free convection magnetohydrodynamic heat and mass transfer from a stretching surface to a saturated porous medium with Soret and Dufour effects, *Computational Materials Science*, 46, 1, 57-65 (2009).

[42] O. Anwar Bég, V. R. Prasad, B. Vasu, N. Bhaskar Reddy, Q. Li and R. Bhargava, Free convection heat and mass transfer from an isothermal sphere to a micropolar regime with Soret/Dufour effects, *Int. J Heat and Mass Transfer*, 54, 9-18 (2011).

[43] P. De, Soret-Dufour Effects on unsteady flow of convective Eyring-Powell magneto nanofluids over a semi-infinite vertical plate, *BioNanoScience*, 9, (1) 7–12 (2019).

[44] R. Viskanta R., Radiation heat transfer in materials processing and manufacturing. In: *Bejan A., Vadász P., Kröger D.G. (eds) Energy and the Environment. Environmental Science and Technology Library*, vol 15. Springer, Dordrecht (1999).

[45] O. Anwar Bég, S. Kuharat, M. Ferdows, M. Das, A. Kadir, M. Shamshuddin, Magnetic nano-polymer flow with magnetic induction and nanoparticle solid volume fraction effects: *solar magnetic nano-polymer fabrication simulation, Proc. IMechE-Part N: J Nanoengineering, Nanomaterials and Nano-systems* (2019). DOI: 10.1177/ 2397791419838714 (19 pages)

[46] O. Anwar Bég, Nonlinear multi-physical laminar nanofluid bioconvection flows: Models and computation, *A. Sohail, Z. Li (Eds.): Computational Approaches in Biomedical Nano-Engineering, Wiley,* Chapter 5, pp. 113-145 (2018). ISBN: 3527344721, 9783527344727.

[47] O. Anwar Bég, Numerical methods for multi-physical magnetohydrodynamics, Chapter 1, pp. 1-112, *New Developments in Hydrodynamics Research, M. J. Ibragimov and M. A. Anisimov, Eds., Nova Science, New York, September* (2012).

[48] R. Viskanta and T. L. Bergman, Heat transfer in materials processing, Warren M. Rohsenow; James P. Hartnett; Young I. Cho (Editors): *Handbook of Heat Transfer*., McGraw-Hill, New York, (1998).

[49] Gebhart *et al*., *Buoyancy-induced Flows and Transport*, Hemisphere, Washington, USA (1988).

[50] E. Magyari and A. Postelnicu, Double diffusive natural convection flows with thermosolutal symmetry in porous media in the presence of the Soret-Dufour effects, *Transport in Porous Media*, 88, 149-167 (2011).

[51] S. Kuharat, O. Anwar Bég, A. Kadir and M. Shamshuddin, Computational study of heat transfer in solar collectors with different radiative flux models, *Heat Transfer Asian Research,* 1-30 (2019). DOI: 10.1002/htj.21418 (30 pages)

[52] Rashid Mehmood, S. Rana, O. Anwar Bég and A. Kadir, Numerical study of chemical reaction effects in magnetohydrodynamic Oldroyd-B oblique stagnation flow with a non-Fourier heat flux model, *J. Brazilian Soc. Mech Sci. Eng.* (2018). https://doi.org/10.1007/s40430-018-1446-4 (14 pages).

[53] K. Madhavi, V.R. Prasad, A. SubbaRao, O. Anwar Bég and A. Kadir, Numerical study of viscoelastic micropolar heat transfer from a vertical cone for thermal polymer coating, *Nonlinear Engineering* (2018). *(13 pages) DOI.ORG/10.1515/NLENG-2018-0064 REC*

[54] M. Hassan, M. Marin, R. Ellahi and S. Z. Alamri, Exploration of convective heat transfer and flow characteristics synthesis by Cu-Ag/water hybrid-nanofluids, *Heat Transfer Research*, 49 (18), 1837-1848 (2018).

[55] M.I.A. Othman and M. Marin, Effect of thermal loading due to laser pulse on thermoelastic porous medium under G-N theory, *Results in Physics*, 7, 3863-3872 (2017).